

FORMATION OF EARLY-TYPE GALAXIES FROM COSMOLOGICAL INITIAL CONDITIONS

THORSTEN NAAB^{1,2}, PETER H. JOHANSSON², JEREMIAH P. Ostriker^{2,3} & GEORGE EFSTATHIOU²

¹ Universitäts-Sternwarte München, Scheinerstr. 1, D-81679 München, Germany; naab@usm.lmu.de

² Institute of Astronomy, Madingley Road, Cambridge CB3 0HA, UK

³ Department of Astrophysics, Peyton Hall, Princeton, USA

Not to appear in Nonlearned J., 45.

ABSTRACT

We describe high resolution Smoothed Particle Hydrodynamics (SPH) simulations of three approximately M_* field galaxies starting from Λ CDM initial conditions. The simulations are made intentionally simple, and include photoionization, cooling of the intergalactic medium, and star formation but not feedback from AGN or supernovae. All of the galaxies undergo an initial burst of star formation at $z \approx 5$, accompanied by the formation of a bubble of heated gas. Two out of three galaxies show early-type properties at present whereas only one of them experienced a major merger. Heating from shocks and -PdV work dominates over cooling so that for most of the gas the temperature is an increasing function of time. By $z \approx 1$ a significant fraction of the final stellar mass is in place and the spectral energy distribution resembles those of observed massive red galaxies. The galaxies have grown from $z = 1 \rightarrow 0$ on average by 25% in mass and in size by gas poor (dry) stellar mergers. By the present day, the simulated galaxies are old (≈ 10 Gyrs), kinematically hot stellar systems surrounded by hot gaseous haloes. Stars dominate the mass of the galaxies up to ≈ 4 effective radii (≈ 10 kpc). Kinematic and most photometric properties are in good agreement with those of observed elliptical galaxies. The galaxy with a major merger develops a counter-rotating core. Our simulations show that realistic intermediate mass giant elliptical galaxies with plausible formation histories can be formed from Λ CDM initial conditions even without requiring recent major mergers or feedback from supernovae or AGN.

Subject headings: galaxy formation: general — galaxy formation: elliptical — methods: numerical

1. INTRODUCTION

There are many puzzles encountered in understanding the formation and evolution of elliptical galaxies and the spheroidal components of spiral galaxies. On the one hand a naive reading of the hierarchical theory of structure formation in a Λ CDM universe would argue that, since massive halos form later than less massive ones, massive ellipticals which reside in the centers of these massive halos should also form late. But there is strong observational evidence that old, massive, red and metal rich proto-ellipticals are already in place at $z = 2 - 3$ and that present day early-type galaxies formed most of their stars well before a redshift $z = 1$ (Searle et al. 1973; Brinchmann & Ellis 2000; Treu et al. 2005; van der Wel et al. 2005). We also know from evidence dating to the 1970's that current rates of star formation in these systems are quite low, the rates increasing sharply into the past as z^1 (Butcher & Oemler 1978; Dressler 1980; Rakos & Schombert 1995). Further, with regard to the evolution of this population, there appears to be a significant increase in the total stellar mass in these old objects from $z = 1$ to the present (Bell et al. 2004; Drory et al. 2004; Conselice et al. 2005; Faber et al. 2005), but this cannot easily be accounted for by the fading of younger, bluer star forming galaxies present at $z = 1$ (Drory et al. 2004; Faber et al. 2005). This has led to the plausible and popular idea that 'dry merging' (i.e. merging of predominantly stellar systems) among elliptical systems (Tran et al. 2005; van Dokkum 2005; Bell et al. 2006b,a) pushes more and more of the mass over the observational cutoff to provide an increased number of $0.5-2L_*$ galaxies.

This attractive idea gives reasonable explanations for some observed correlations of the mass of ellipticals and their kinematics, sizes or isophotal shape (Khochfar & Burkert 2005; Naab et al. 2006b; Boylan-Kolchin et al. 2006). However, noting that there are tight relations among luminosity, color, age and metallicity, puts severe limits on the amount of late dry merging that could acceptably occur without destroying the aforementioned constraints.

On the theoretical side it is now possible to perform accurate high resolution simulations of the gravitational evolution of the dark matter distribution (Moore et al. 1998; Springel et al. 2005b). In contrast, the numerical simulation of galaxy formation, including a hydrodynamic treatment of the baryonic component, is still in its infancy. Very few high resolution simulations from realistic cosmological initial conditions have been done so far and most of these have concentrated on the formation of disc galaxies rather than early-type spheroidal systems (Sommer-Larsen et al. 2003; Abadi et al. 2003; Governato et al. 2004; Robertson et al. 2004).

This is surprising since spheroidal systems are of interest in their own right, as they contain more than half of the total stellar mass in the local universe (Fukugita et al. 1998). The most massive galaxies known, the giant ellipticals, are spheroidal systems which predominantly consist of old stars (see e.g. Thomas et al. 2005a) and so must have formed at high redshift. They are therefore likely to be good probes of galaxy assembly, star formation and metal enrichment in the early Universe.

Most numerical work on early-type galaxy forma-

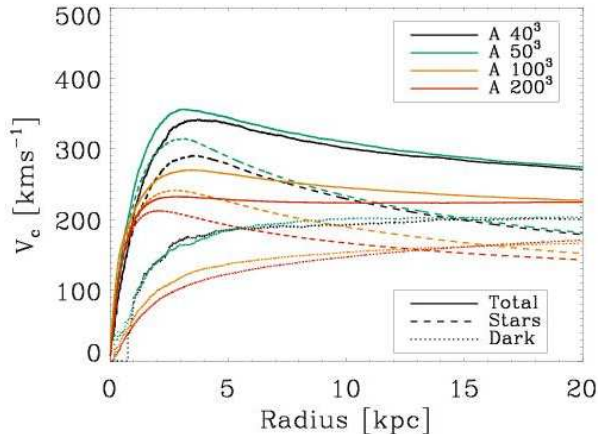


FIG. 1.— Circular velocity curves for galaxy A at four different numerical resolutions: 40^3 , 50^3 , 100^3 , and 200^3 SPH particles and collisionless dark matter particles, respectively. Note how the rotation curves become increasingly flat as the resolution increases.

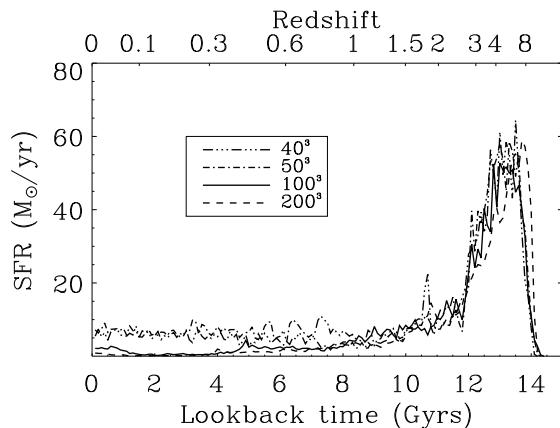


FIG. 2.— Star formation rate (SFR) histories, computed from stellar ages, of galaxy A versus lookback time at four different numerical resolutions: 40^3 , 50^3 , 100^3 , and 200^3 SPH particles and collisionless dark matter particles, respectively. There is a strong trend that the low redshift star formation rate is reduced in higher resolution simulations.

tion has used either very idealized initial conditions (Kobayashi 2004), or had insufficient spatial and mass resolution to resolve the internal structures of galaxies (Kawata & Gibson 2003; Sáiz et al. 2004). An exception is the simulation discussed by Meza et al. (2003). These authors used an SPH simulation that included feedback from supernovae to follow the formation of a single spheroidal galaxy self-consistently from CDM initial conditions. The spatial resolution of this simulation was high enough to resolve the region within an effective radius for a typical real elliptical galaxy. However, the final stellar system formed in this simulation was far too dense, with an effective radius about an order of magnitude smaller than real elliptical galaxies of the same brightness. Meza et al. (2003) speculate that this discrepancy may be a consequence of their star formation and feedback algorithm and that it might be possible to produce less concentrated systems if more aggressive stellar feedback were implemented to prevent star formation in high density sub-units at high redshift.

In this paper we present high resolution hydrodynamical simulations based on cosmological initial conditions admitting, intentionally, only bare-bones prescriptions for the physics involved (e.g. no “feedback” from supernovae or AGN), to see if some resolution of these paradoxes can be derived. The rationale for simplifying the simulations is straightforward. As we will show in Section 3, at least 100^3 gas particles are required for hydrodynamical simulations to ‘converge’, making them very expensive to run. With present generation computers it is impossible to run a large ensemble of simulations of this size to properly explore a huge parameter space. Our point of view, therefore, is to keep the physics of the simulations as simple as possible and to get an understanding of the behaviour of a simplified problem before investigating additional complexities such as supernova and AGN feedback. Our goal in this paper, therefore, is to investigate the formation of a number of massive ($\approx M_*$) isolated galaxies starting from realistic initial conditions and to see how variable the final systems and whether they resemble real galaxies.

What we find can be summarized simply. The initial cooling and collection of cold gas from infalling smaller scale perturbations happens very rapidly and easily within the most massive systems leading to a very rapid burst of star formation beginning at $z \sim 6$ and then falling off exponentially on a time-scale of roughly 1.5 Gyrs. This phase is terminated as the star forming region is enveloped in an expanding hot bubble which prevents new, infalling cold gas mass elements from reaching the central regions. This early phase - reminiscent in some respects to a modernized version of the “monolithic collapse” picture of galaxy formation, prominent in the 1960’s through 1980’s (Larson 1974; van Albada 1982)- produces a sequence of objects with effective radii of 1-2 kpc, which might satisfy the tight relations observed among the red metal rich old cores of elliptical galaxies.

For simulations with early-type properties at $z = 0$ stellar accretion or mergers (the choice of the appropriate term for the process is arbitrary and dependent on the relative mass of the infalling stellar objects) add to the growing stellar envelope of relatively blue, old and metal poor stars. This accounts for the growth in size seen for ellipticals as well as the growth in total mass in the time frame $z = 1 \rightarrow 0$. Furthermore, since this assembly of added stellar mass is not accompanied by much in situ star formation (the coterminously added hot and cold gas being simply added to the expanding hot bubble surrounding the central galaxy) the growth of the stellar population occurs without the presence of young stars. Existing work has shown that the tightness of the elliptical color-magnitude relation puts strong constraints on dry merger scenarios (Bower et al. 1998; Kaviraj et al. 2005). But we find that in our simulations that minor mergers or accretion events do not typically add much stellar mass to the central region, because of the relatively large angular momentum of the infalling systems - and thus the central, tight color-magnitude relations are not expected to be overly perturbed even if as much as 40% of the total final mass is added during this phase. As an additional byproduct of this assembly scenario, we find it readily understandable how so much of the stellar mass in these systems resides in regions of such low density, where star formation would always have been diffi-

cult to contemplate. The stars seen at $R \sim R_e$ were not born there, but rather were formed in the central regions of much lower mass systems that have been accreted and shredded in the envelopes of the giant elliptical galaxies.

2. INITIAL CONDITIONS AND SIMULATIONS

The initial conditions of the Λ CDM simulation assumed scale-invariant adiabatic fluctuations. The post-recombination power spectrum for the CDM cosmology was based on the parameterization of Efstathiou et al. (1992) with $\Gamma=0.2$. We use a WMAP1 (Spergel et al. 2003) cosmology with a slightly lower Hubble parameter of $h = 0.65$ ($\equiv H_0=100h \text{ kms}^{-1}\text{Mpc}^{-1}$) with $\sigma_8=0.86$, $f_b = \Omega_b/\Omega_m=0.2$, $\Omega_0=0.3$, and $\Lambda_0=0.7$.

In a low resolution, dark matter simulation (128^3 dark matter particles with a box size of $L_{box} = 50$ Mpc using the (AP³M) N-body code of Couchman (1991)). We selected virialized halos with masses in the range $7 \times 10^{11} M_\odot < M_{halo} < 3 \times 10^{12} M_\odot$ in a low density environment such that the nearest halo with $M_{halo} > 2 \times 10^{11} M_\odot$ is more than one Mpc/h away. To re-simulate the target halos at high resolution we increased the particle number to 100^3 gas and dark matter particles within a cubic volume at redshift $z = 24$ containing all particles that end up within the virialized region (conservatively we assumed a fixed radius of 0.5 Mpc) of the halos at $z = 0$. From this sample we have selected three systems with final stellar masses of $\approx M_*$ for elliptical galaxies in the range of $9.6 \times 10^{10} M_\odot < M < 1.6 \times 10^{11} M_\odot$ (Cole et al. 2001; Kochanek et al. 2001; Bell et al. 2003) for the cosmology chosen here. For one halo (halo A) the resolution was increased to 200^3 particles. Additional short wavelength perturbations were included to account for the missing small-scale power below the Nyquist frequency of the low resolution simulation. The tidal forces from particles outside the high resolution cube were approximated by increasingly massive dark matter particles in 5 nested layers of lower and lower resolution. None of the galaxies was contaminated by boundary particles within their virial radii.

The simulations were run with GADGET-2 (Springel 2005) on COSMOS, a shared-memory Altix 3700 with 1.3-GHz Itanium2 processors hosted at the Department of Applied Mathematics and Theoretical Physics (Cambridge) and on two similar machines at Princeton University and the University Observatory in Munich. We used a fixed comoving softening until $z = 9$, and after this the softening remained fixed at the same values in physical coordinates. The simulation parameters for each halo are given in Tab.3. The amount of stars formed for each gas particle is proportional to the mass of the star forming gas component and inversely proportional to the star formation timescale t_* . This timescale is $t_* = t_0^* \sqrt{\rho_{crit}/\rho}$, where t_0^* is the characteristic star formation timescale which we set to $t_0^* = 1.5$ Gyr (Springel & Hernquist 2003). Within a factor of a few the exact value of t_0^* does not change the results.

The density threshold for the onset of star formation was set to $\rho_{crit} = 7 \times 10^{-26} \text{ g cm}^{-3}$ following Navarro & White (1993). In addition we require an overdensity contrast of $\Delta > 55.7$ for the onset of star formation in order to avoid spurious star formation at high redshift. We included an uniform UV background radiation field of a modified Haardt & Madau (1996) spectrum,

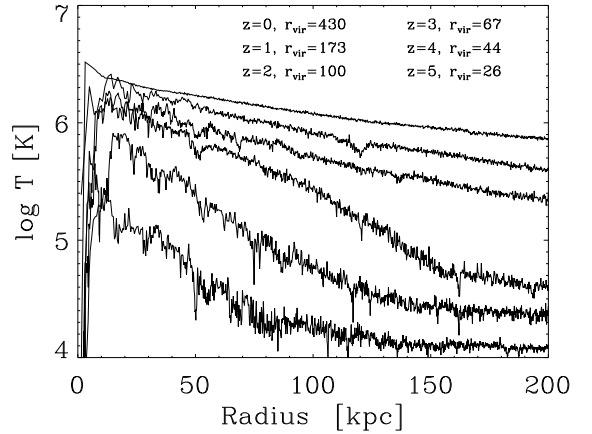


FIG. 3.— Time evolution of the gas temperature profile from $z = 5$ to $z = 0$ (from bottom to top) for halo A (200^3 resolution). The average temperature of the gas is steadily increasing. At the end of its initial formation phase at $z \approx 2$ the galaxy is surrounded by a halo of hot gas heated to the virial temperature.

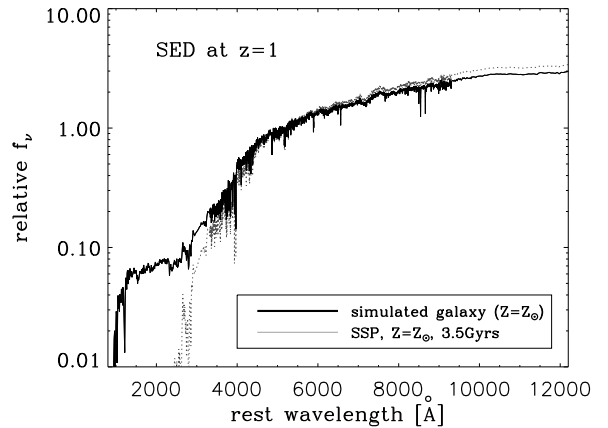


FIG. 4.— Spectral energy distribution (SED) of the galaxy A (200^3) at $z = 1$ (black line) with solar metallicity for all stars. We have assumed that stars younger than 10^7 yrs are obscured. For comparison we show the SED for a 3.5 Gyrs old simple stellar population (SSP) with solar metallicity (grey dotted line) using the Bruzual & Charlot (2003) models with a Salpeter IMF.

where reionization takes place at $z \simeq 6$ (Davé et al. 1999) and the intensity of the UV background field peaks at $z \simeq 2-3$. Following Katz et al. (1996) the radiative cooling and heating rates were computed assuming that the gas is optically thin and in ionization equilibrium. The self-shielding of star-forming clouds from the UV flux (e.g. Susa & Umemura 2000; Zheng & Miralda-Escudé 2002) was not included in the simulations. The abundances of the different ionic hydrogen and helium species were then computed by solving the network of equilibrium equations self-consistently for a specified value of the UV background radiation field. The late star formation history is relatively insensitive to minor changes in the UV background field, whereas an increase in the UV background at high redshift might soften the star formation peak. A detailed investigation of the effect of the UV background on the simulations presented here will be discussed in a future paper.

3. A MASSIVE GALAXY AT Z=1

TABLE 1
PROPERTIES OF GALAXY A AT $r < r_{\text{vir}}$

Resolution	M_{vir} ^(a)	M_{stars}	M_{gas}	M_{dark}	r_{vir} ^(b)	v_{max} ^(c)	m_{stars} ^(d)	m_{dark}	ϵ_{stars} ^(e)	ϵ_{dark}
40^3	242	25.3	20.2	197	434	341	161	1288	0.625	1.3
50^3	241	27.0	20.1	193	433	356	82.5	659	0.5	1.0
100^3	230	23.8	20.9	184	427	270	10.5	82	0.25	0.5
200^3	225	24.9	18.4	182	424	232	1.3	10.3	0.125	0.25

NOTE. — (a) Total masses M in $10^{10} M_{\odot}$; (b) Virial radius in kpc; (c) Maximum circular velocity in km/s; (d) Particle masses m in $10^5 M_{\odot}$; (e) Gravitational softening lengths in kpc

TABLE 2
PROPERTIES OF GALAXY A AT $r < 30\text{KPC}$

Resolution	M_{stars} ^(a)	M_{gas}	M_{dark}
40^3	16.3	1.0	27.7
50^3	16.6	1.0	28.7
100^3	12.2	0.6	20.4
200^3	11.8	0.5	23.1

NOTE. — (a) Total masses M in $10^{10} M_{\odot}$

To investigate the effect of numerical resolution on the cosmological simulation of an individual galaxy we have simulated our primary example, halo A, at four different resolutions using 40^3 , 50^3 , 100^3 and 200^3 SPH particles and the same number of dark matter particles, respectively. The simulation parameters are given in Tab. 1.

The virial radius and the enclosed total mass in baryons and dark matter of the galaxy changes weakly with increasing resolution (see Tab. 1). However, the amount of baryons concentrated to the central 30 kpc at the higher resolutions is reduced by more than 20% compared to the lowest resolution (see Tab. 2). In addition the circular velocity profiles $v_c^2 = GM(r)/r$ become flatter with increasing resolution and the peaks are shifted to smaller radii (Fig. 1).

The detailed star formation history of the galaxies also changes with numerical resolution. In Fig. 2 we compare the SFR histories of the 40^3 , 50^3 , 100^3 , and 200^3 simulations. The numerical resolution has a weak influence on the SFR at redshifts higher than $z = 1$. In all cases the SFRs peak at $z \approx 5$ at rates of $\approx 60 M_{\odot}/\text{yr}$. However, at the 200^3 resolution the peak of the SFR is shifted to higher redshifts. At redshifts below $z = 1$ the low resolution galaxies, e.g. 40^3 and 50^3 particles, have significantly higher star formation rates (and gas fractions, see Tab. 2) than the 100^3 and the 200^3 simulation which has the lowest present day star formation rate. The higher star formation rates (and larger final baryon fractions) of the low resolution simulations are caused by a continuing infall of cold gas, even at low redshifts. It has been shown by Agertz et al. (2006) and Junk et al. (2006) that SPH, especially at low resolution, has a limited ability to resolve Kelvin-Helmholtz instabilities: Instead of being destroyed a cold gas cloud moving in a hot gaseous halo can be artificially stabilized and sink all the way to the center. In our simulations this artificial effect is suppressed at higher resolution as the infalling clumpy gas is better resolved and can be stripped and dispersed in the hot gaseous halo of the host galaxy.

A comparison simulation at the 100^3 resolution with a longer star formation time-scale of $t_0^* = 4.5$ Gyr is similar to the $t_0^* = 1.5$ Gyr simulation at high redshifts but shows significantly less star formation at low redshift. These results implicate that the resolution has a strong

effect and the actual choice of the time-scales has a weak effect on the galaxy properties. As the present day color of the galaxy is very sensitive to recent star formation it is very problematic to use it as a diagnostic tool without considering other galaxy properties.

We have used the highest resolution (200^3) simulation to study the star formation in some more detail. The stars form in clumps of cold gas that have collapsed on small scales. As the cold gas is depleted, the SFR declines rapidly. The diffuse gas in the forming halo, which does not reside in cold sub-clumps, is heated by shocks and forms an expanding bubble of hot gas which reaches virial temperature at $2 < z < 3$. As an example we show the evolution of the gas temperature of halo A in Fig. 3. Although during this phase the cooling time of the hot gas is shorter than the Hubble time, the heating time of the infalling gas is even shorter (Ciotti & Ostriker 2001; Birnboim & Dekel 2003; Sazonov et al. 2005; Dekel & Birnboim 2006). After $z = 2$ there is an increasing contribution to heating from -PdV work and entropy addition via weak shocks which becomes dominant towards $z = 0$. In this paper we focus on the assembly history and the observable properties of the simulated systems. A full quantitative analysis of the heating processes is beyond the scope of this paper and will be presented in Johansson et al. (2006, in preparation).

Galaxy A (200^3) has assembled 80% of its final stellar mass by $z = 1$ (see Section 4). At this time the stellar mass within 30 kpc (we use this fiducial value as the stars in ellipticals typically can not be observed at larger radii) is $M_* = 9.8 \times 10^{10} M_{\odot}$ and the mean age of the stellar population is 3.9 Gyrs. We constructed the spectral energy distribution (SED) of the galaxy at $z = 1$ using the spectro-photometric stellar evolution models of (Bruzual & Charlot 2003) assuming a mean stellar metallicity close to solar $Z = Z_{\odot} = 0.02$ and a Salpeter IMF (Fig. 4). Qualitatively the SED does not change for small changes in metallicity. We also assumed that recently formed stars younger than 10^7 yrs are obscured and do not contribute to the total flux. No further corrections for reddening, e.g. for absorption by dust, have been applied. The SED looks remarkably similar to rest-frame SEDs of ERO's (Moustakas et al. 2004). However, in the absence of reddening corrections, the redshift corrected observed colors are not quite extreme enough at $R - K = 4.6$ and $I - K = 3.2$. With an observed magnitude of $m_K = 19.3$ and the above red colors the object could alternatively be classified as a Very Red Object, see e.g. (McCarthy 2004; Väisänen & Johansson 2004).

4. ASSEMBLY HISTORIES FOR THREE GALAXIES

The similarity in the star formation and assembly history as well as in the present day properties of the 100^3

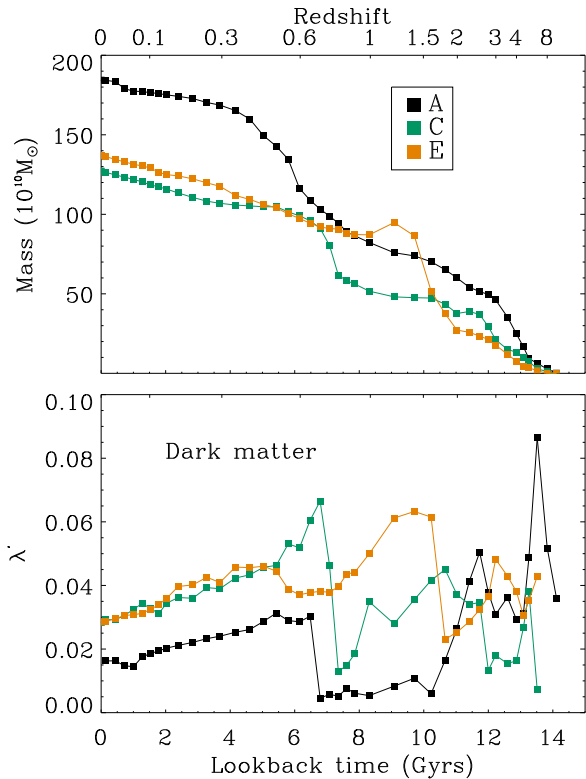


FIG. 5.— *Top*: Dark matter mass accretion history of the three (100^3) halos within their virial radii. Halo E accretes smoothly after $z = 1$. *Bottom*: Evolution of the halo spin parameter λ' . The merger events for halos A and C at $z \approx 0.7$ can be clearly identified by the sudden increase of the spin.

and 200^3 simulations for galaxy A encouraged us to believe that at a resolution of 100^3 particles (and the corresponding spatial and mass resolution) the simulations are numerically well enough resolved to run more halos and find out whether the above results are typical. With current hardware and software it is difficult to run many halos at 200^3 or even higher resolution.

The dark matter mass accretion history and the spin evolution of the three halos is shown in Fig. 5. We computed the mass within the virial radius defined by an enclosed mean overdensity of 200. By $z = 1$ halos A and C have gained $\approx 40\%$ of their final mass. Thereafter the halos continue to accrete dark matter and halo A has a merger with a mass ratio of 6.5:1 at $z \approx 0.6$, halo C has a major merger with a mass ratio of 3.5:1 at $z \approx 0.8$. Halo E has already assembled more than 60% of its mass by $z = 1$ and undergoes an almost equal-mass merger at $z = 1.6$. Thereafter the halos grow until $z = 0$ without any indication for a significant merger event. No halo experienced a major merger within the last 4 Gyrs.

The evolution of the halo spin parameter λ' defined as

$$\lambda' = \frac{J}{\sqrt{2}M_{\text{vir}}v_c r_{\text{vir}}}, \quad (1)$$

where v_c is the circular velocity at the virial radius r_{vir} and M_{vir} is the virial mass (Bullock et al. 2001), is shown in the bottom plot of Fig. 5. Halo E had gained significant spin during the $z = 1.6$ major merger event which can clearly be identified by the sudden jump in λ' . This merger induced increase of spin is in agreement with the findings of Vitvitska et al. (2002) based on dark

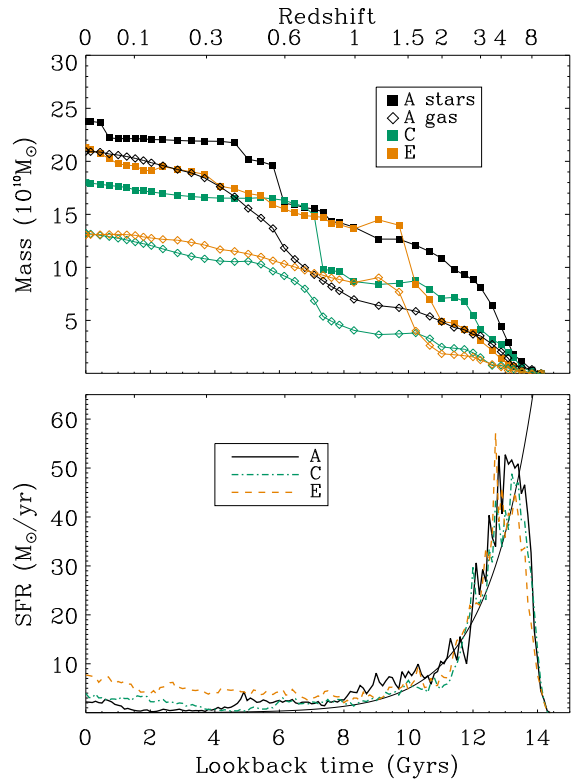


FIG. 6.— *Top*: Baryonic mass accretion history within the virial radius of the galaxies subdivided in stars and gas. *Bottom*: Star formation rate histories computed from stellar ages at $z = 0$. The dashed line indicates an evolution $\propto \exp(-(t - t_0)/\tau)$ with $t_0 = 14.5$ Gyrs and $\tau = 1.5$ Gyrs for comparison.

matter simulations. By $z = 1$ the spin of halo E is larger than $\lambda' = 0.05$ and decreasing smoothly towards $\lambda' = 0.03$ at $z = 0$. In contrast, Halos A and C have low spin at $z = 1$ and thereafter gain significant spin during the merger events. The final spin values of all halos, $\lambda' < 0.04$, is below the average predicted by dark matter simulations, however, their time evolution is consistent (Vitvitska et al. 2002).

In the top row of Fig. 6 we show the accretion history of the baryonic matter subdivided into gas and stars within the virial radius of each halo. Halo A has assembled most of its stellar mass by $z = 1$ whereas halos C and E grow significantly at lower redshifts. By $z = 0$ halo A has almost half of the baryons in gas with a ratio of stellar mass to gas mass of $M_{\text{stars}}/M_{\text{gas}} = 1.1$. Halo E, at a similar mass, has significantly more baryons in stars with $M_{\text{stars}}/M_{\text{gas}} = 1.6$. We derive the star formation rate (SFR) histories of the galaxies (bottom plot of Fig. 6) using the stellar ages at $z = 0$ of all stars within 30 kpc (again, we use this fiducial value as the stars in ellipticals typically can not be observed at larger radii). All galaxies start forming their stars in a burst at $z \approx 3 - 5$ with peak SFRs of $\approx 40 - 60 M_{\odot}/\text{yr}$ and undergo an intense phase of merging (see the random walk of the halo spin parameters in Fig. 5) during which the SFRs decline exponentially towards $z = 1$. At $z = 1$ the galaxies sustain star formation at rates of $3 - 7 M_{\odot}/\text{yr}$. For halos A and C the star formation rate drops to zero soon after their last merger event. About 2 Gyrs later small amounts of the previously heated gas is cooling at the center of these galaxies and the SFR is rising again

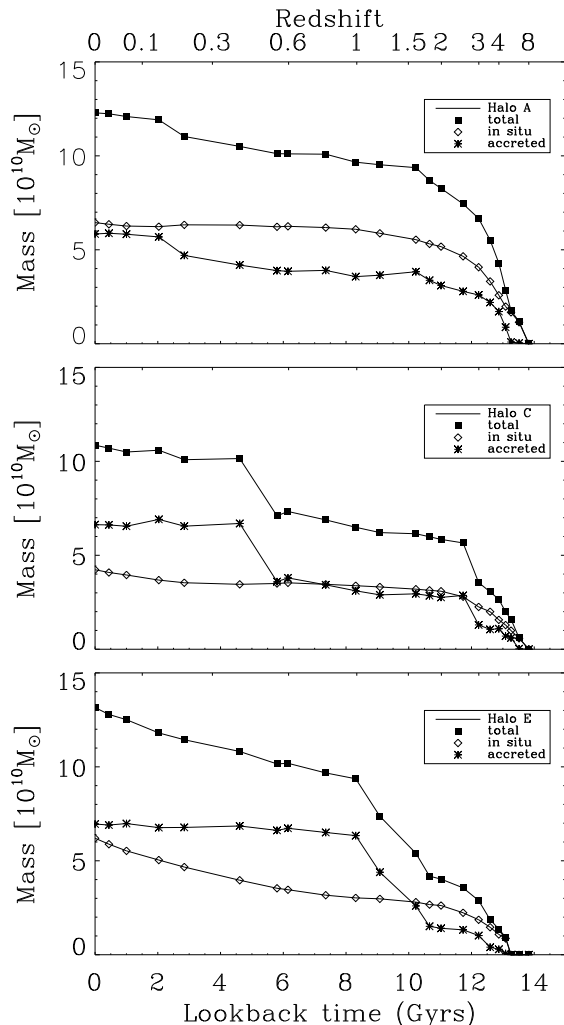


FIG. 7.— Accretion history for galaxies A, C and E of stars that have been added onto the central physical 30 kpc (asterisk), stars that have formed in the galaxy in situ (open diamond) and the sum of the two (filled squares).

to $\approx 2M_{\odot}/\text{yr}$. Halo E, which did not undergo any significant merger after $z = 1$ sustains an almost constant star formation rate until $z = 0$.

The above star formation histories were derived from the present day fossil record of the stars in the galaxies. They indicate the time but not the location the stars were born. The stellar mass of the galaxies is steadily increasing with time both by stars that were born from gas in situ in the galaxy as well as stars that have formed outside the galaxy and later on have been accreted. In Fig. 7 we show the time evolution of stellar mass within a fixed physical radius of 30kpc separated into stars that were born within the galaxies and stars that have been accreted. By $z = 1$ galaxy A has already assembled 80% of its final stellar mass when about 60% of the stars have formed inside the galaxy whereas 40% have been accreted by mergers. From $z = 1$ to $z = 0$ further mass assembly is dominated by accretion of stars which are accreted in small subunits. The most massive satellite is accreted at $z \approx 0.2$ and, after it has been stripped, has 10% of the mass of the host galaxy. It had originally been accreted onto the halo in the merger event at $z = 0.6$ that is described above. Galaxy C experiences a major $\approx 3:1$

merger at $z = 0.6$. This merger can be identified as a gas poor or dry merger as both progenitors were gas poor and the merger was not accompanied by a burst of star formation (see Fig. 6). Galaxies A and C show on average an increase in mass by ‘dry’ mergers of 24% and only a few percent by in situ star formation from $z = 1 \rightarrow 0$. The situation is different for galaxy E which grows predominantly by in situ star formation from $z = 1 \rightarrow 0$ (see Fig. 9).

In Fig. 8 we show the time evolution of the projected cylindrical half-mass radius (again within fixed physical 30kpc) for the galaxies as a whole and for the in situ and accreted population separately. The stars formed in situ have typical half mass radii of 1-2 kpc which changes only weakly with redshift. The accreted stars have significantly larger half mass radii that lead to an increase of the total half-mass radius for galaxies A, C and E as the accreted mass is increasing towards the present time. The situation is different for galaxy E: the in situ half mass radius is constant as well, however, the mass in situ stars is increasing. As a result the half mass radius of the galaxy is decreasing similar to adiabatic contraction (Blumenthal et al. 1986; Jesseit et al. 2002).

5. PRESENT DAY PROPERTIES

We have summarized the properties inside the virial radius of the galaxies in Tab. 3. In Fig. 10 we show the circular velocity curves for all galaxies normalized to their projected stellar half mass radii. These seem very reasonable, in marked contrast to the results of e.g. Meza et al. (2003). The galaxies are dominated by luminous matter inside 10 kpc and the fraction of dark matter within the half-mass radii is $0.18 < f_{\text{DM}} \approx 0.38$. This is consistent with most findings based on observations and dynamical modeling that early-type galaxies are dominated by luminous matter in their inner parts (Efstathiou et al. 1982; Rix et al. 1997; Romanowsky et al. 2003; Treu & Koopmans 2004; Thomas et al. 2005b). However, dynamical modeling of observed ellipticals also indicates that dark matter becomes dominant beyond 2-3 half-mass radii whereas for the simulated galaxies A, C, and E dark matter becomes dominant at a factor of two larger radii.

The properties of the central stellar component of the galaxies are summarized in Tab. 4. At present galaxies A and C have very old stellar population with mean ages of about 11 Gyrs, galaxy E which had significant recent star formation is more than one Gyr younger. The final stellar masses within 30kpc are in the range of $10.8 \times 10^{10} M_{\odot} < M_{*} < 13.2 \times 10^{10} M_{\odot}$. We have computed the luminosities of the galaxies using the Bruzual & Charlot (2003) spectro-photometric models assuming a Salpeter IMF and solar metallicity. As all galaxies had recent star formation on various levels (see Fig. 6), they are shifted blue-ward from the color magnitude relation of cluster ellipticals (see e.g. McIntosh et al. 2005). However, for galaxies A and C the effect is not very strong and any process that would suppress central star formation within the last 10^8 yrs would shift the galaxies (with the exception of galaxy E) to the observed relation. Higher numerical resolution might result in a similar effect, as galaxy A at 200^3 resolution falls right on the color-magnitude relation. However, it is not unusual for field ellipticals (E+A phenomenon) to actually show residual star for-

TABLE 3
GALAXY PROPERTIES FOR $r < r_{\text{vir}}$

Galaxy	$M_{\text{vir}}^{(a)}$	M_{stars}	M_{gas}	M_{dark}	$r_{\text{vir}}^{(b)}$	$v_{\text{max}}^{(c)}$	$\langle \Lambda' \rangle^{(d)}$	$f_{\text{hot}}^{(e)}$	$m_{\text{stars}}^{(f)}$	m_{dark}	$\epsilon_{\text{stars}}^{(g)}$	ϵ_{dark}
A	229	23.8	20.9	184	426	270	0.022 ± 0.012	0.99	10.5	82.5	0.25	0.5
C	158	18.0	13.2	127	377	257	0.034 ± 0.012	0.99	8.5	69	0.25	0.5
E	171	21.3	13.1	137	387	307	0.039 ± 0.010	0.98	8.5	69	0.25	0.5

NOTE. — (a) Total masses M in $10^{10} M_{\odot}$; (b) Virial radius in kpc; (c) Maximum circular velocity in km/s; (d) Time averaged halo spin parameter; (e) Fraction of hot gas ($T > 10^5$ K); (f) Particle masses m in $10^5 M_{\odot}$; (g) Gravitational softening lengths in kpc

TABLE 4
GALAXY PROPERTIES FOR $r < 30\text{kpc}$

Galaxy	$M_{\text{stars}}^{(a)}$	M_{gas}	$f_{\text{hot}}^{(b)}$	$r_{1/2}^{(c)}$	$\langle \text{age} \rangle_*^{(d)}$	$M_{\text{B}}^{(e)}$	$SB_{\text{eff}}^{(f)}$	$r_{\text{eff}}^{(g)}$	$f_{\text{DM}}^{(h)}$	$\epsilon^{(i)}$	$a_4^{(j)}$	$\sigma_0^{(k)}$	$v_{\text{maj}}^{(l)}$	$\langle H_3 \rangle^{(m)}$	$T^{(n)}$
A	12.3	0.64	0.95	2.2	11.5	-20.18	20.5	2.7	0.38	0.18	0.6	153	43	-0.05	0.08
C	10.8	0.82	0.90	2.5	11.2	-20.45	20.3	2.8	0.35	0.21	1.1	145	84	-0.09	0.77
E	13.2	0.84	0.88	1.4	9.8	-21.06	19.7	1.9	0.18	0.5	2.5	180	225	-0.05	0.13

NOTE. — (a) Total masses M in $10^{10} M_{\odot}$; (b) Fraction of hot gas ($T > 10^5$ K); (c) Projected stellar half-mass radius; (d) Average stellar age at $z=0$; (e) Absolute magnitude in B-band; (f) Effective surface brightness in B-band in mag arcsec^{-2} ; (g) Fitted effective radius; (h) fraction of dark matter within r_{eff} ; (i) Ellipticity at r_{eff} ; (j) Isophotal shape parameter; (k) Central stellar velocity dispersion in km/s; (l) Major axis velocity in km/s; (m) LOSVD asymmetry parameter; (n) Triaxiality parameter

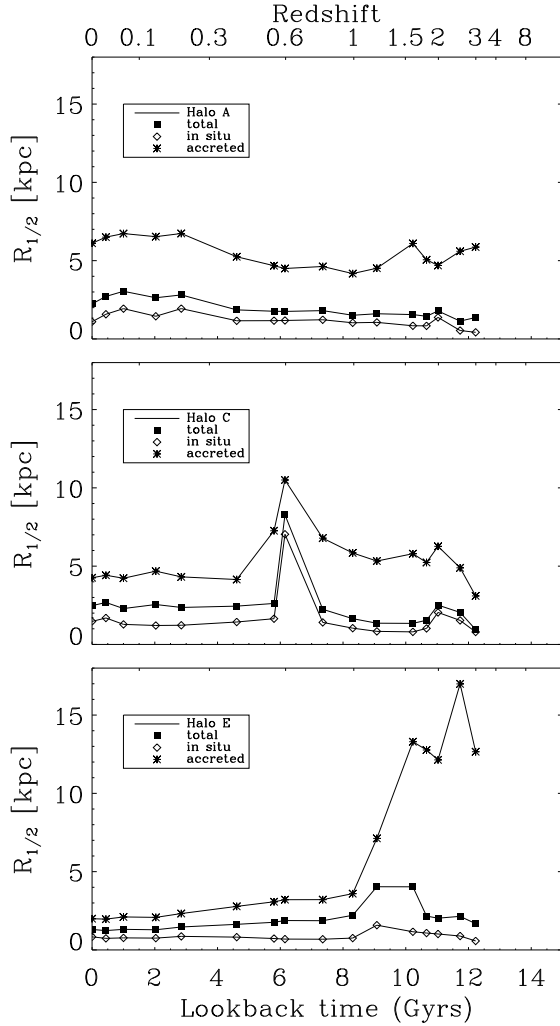


FIG. 8.— Time evolution of the projected spherical half-mass radius for galaxies A,C and E of all stars (filled squares) and the accreted (stars) and in situ stars (open diamonds) within a fixed radius of physical 30 kpc.

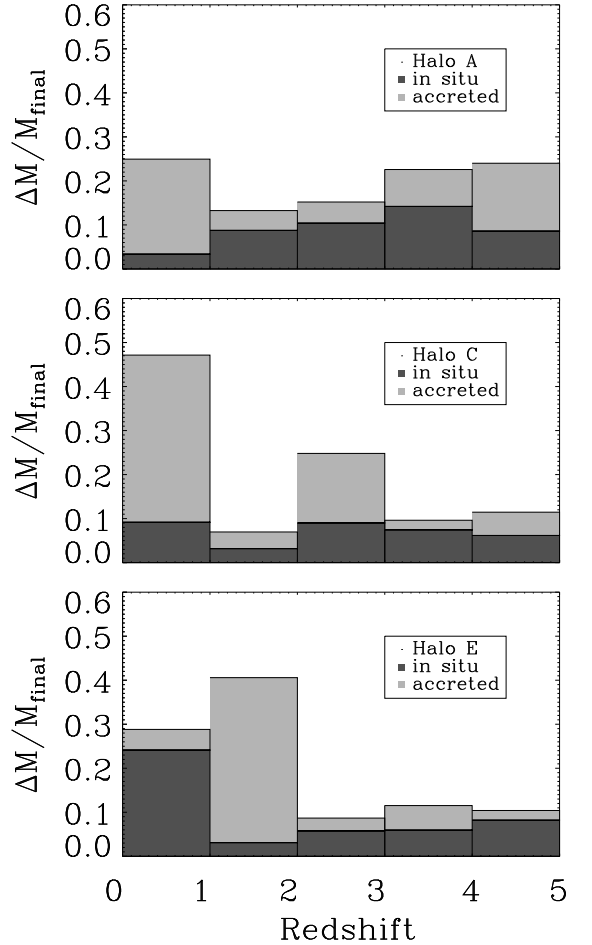


FIG. 9.— Accreted stellar mass and stars formed in situ as a function of redshift for the three galaxies. From $z = 1 \rightarrow 0$ galaxies A and C grow by gas poor mergers whereas galaxy E grows by in situ star formation.

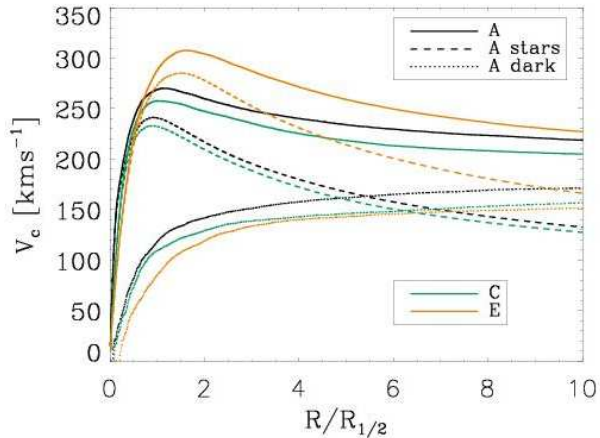


FIG. 10.— Circular velocity curves for all galaxies versus radius normalized to their projected stellar half-mass radius. All galaxies are dominated by luminous matter inside two half-mass radii.

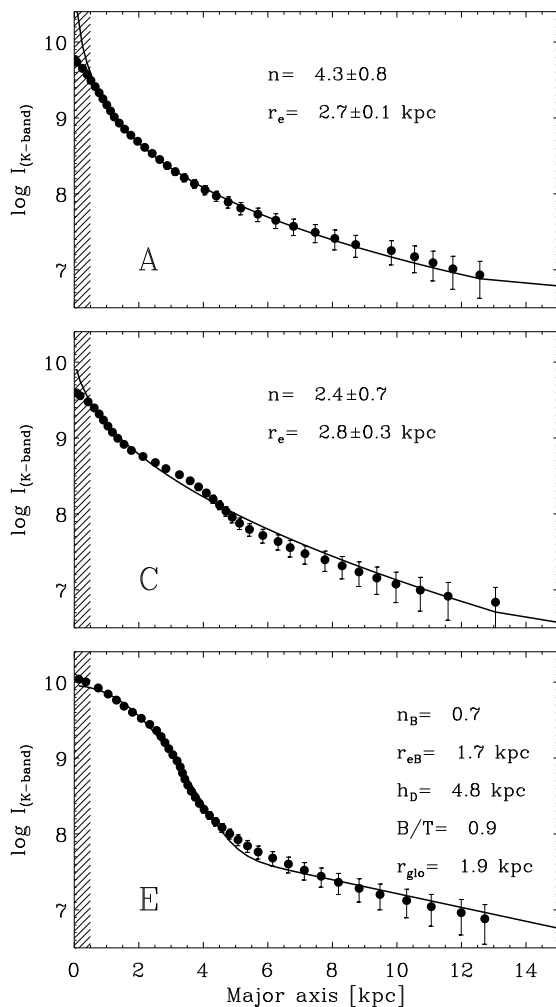


FIG. 11.— K-band surface brightness profiles for galaxies A, C, and E. The profiles inside ≈ 2 softening lengths (shaded area) were excluded from the fits as they are likely to be influenced by force softening. The error bars are given by the Poissonian error of the particles in the fitted regime. The errors for the Sérsic index n and the effective radius r_e have been determined by the bootstrapping method. Galaxies A and C can be fitted well by a single Sérsic function whereas galaxy E can only be fitted by a two component fit (see text).

mation (Blake et al. 2004; Schawinski et al. 2006).

The simulations had sufficient resolution (a few 10^5 particles within 30kpc) to analyze the kinematic and photometric properties in more detail. In Fig. 11 we show the edge-on K-band surface brightness profiles of the galaxies and the best fitting Sérsic function or the best two component Sérsic+exponential fit (Naab & Trujillo 2006). With Sérsic indices of $n = 4.3$ and $n = 2$ and effective radii of 2.7 kpc and 2.8 kpc galaxies A and C can best be fitted by a single Sérsic function and have a very reasonable concentration in good agreement with observed intermediate mass ellipticals (Trujillo et al. 2004). Galaxy E can not be fitted with a single component. It is dominated by a central 'bulge' component with a Sérsic index of $n_B = 0.5$ and a size of $r_{eB} = 1.7\text{kpc}$ and an outer exponential with a scale length of $h_d = 4.8\text{kpc}$. The bulge-to-total ratio is $B/T = 0.9$. In fact the central component is a compact exponential disk seen edge-on.

We have investigated the LOSVDs of the galaxies by binning the velocities on a slit along the apparent long axis of each projected galaxy. Subsequently we parameterized deviations from the Gaussian shape using Gauss-Hermite basis functions (Gerhard 1993; van der Marel & Franx 1993). The kinematic parameters of each profile (v_{fit} , σ_{fit} , h_3 , h_4) were then determined by least squares fitting as in Naab et al. (2006a). As an example we show the fitted kinematical profiles for the edge on projection of galaxies A and C in Figs. 12 and 13. As they are affected by higher order moments we show the real line-of-sight velocity and dispersion in addition (dashed lines). Both galaxies show significant rotation. Galaxy C has a counter-rotating core that has formed during the major merger event. The velocity dispersion profiles are peaked towards the central region and drop in the outer parts. The drop at the very center is caused by stars that have formed late from the cooled halo gas. A similar behavior is seen in some field ellipticals like, e.g. NGC2768 (Emsellem et al. 2004) and could have the same origin. The asymmetry of the LOSVD measured by h_3 is always anti-correlated to the line-of-sight velocity, whereas the LOSVD is more peaked than a Gaussian at the center, indicated by a positive value of h_4 . The errors have been computed applying the bootstrap algorithm. Even for the higher order moments they are reasonably small within the effective radius.

In Fig. 14 we show the location of 500 random projections of galaxies A, C, and E in the $v_{\text{fit}}/\sigma_{\text{fit}}-h_3$ plane. The shaded area indicate the 90% probability to find projected galaxy with the given properties. All projected galaxies show steep leading wings in their LOSVD (anti-correlated h_3 and v_{fit}). The location of the galaxies is in good agreement with observations of elliptical galaxies indicated by the symbols in Fig. 14 (Bender et al. 1994; Naab et al. 2006a). Galaxy E is the fastest rotator with $v_{\text{fit}}/\sigma_{\text{fit}} \approx 2$.

We determined the characteristic ellipticity ϵ_{eff} , the isophotal shape $a4_{\text{eff}}$ ($a4_{\text{eff}} < 0$: boxy isophotes; $a4_{\text{eff}} > 0$: disk isophotes) as well as the central velocity dispersion σ_0 , the maximum rotation velocity v_{maj} , and the triaxiality parameter T as in Naab & Burkert (2003). In Fig. 15 we indicate the location of the simulated galaxies A, C, and E in the plane defined by the anisotropy parameter $v_{\text{maj}}^*/\sigma_0$ and the isophotal shape $a4_{\text{eff}}$. We have

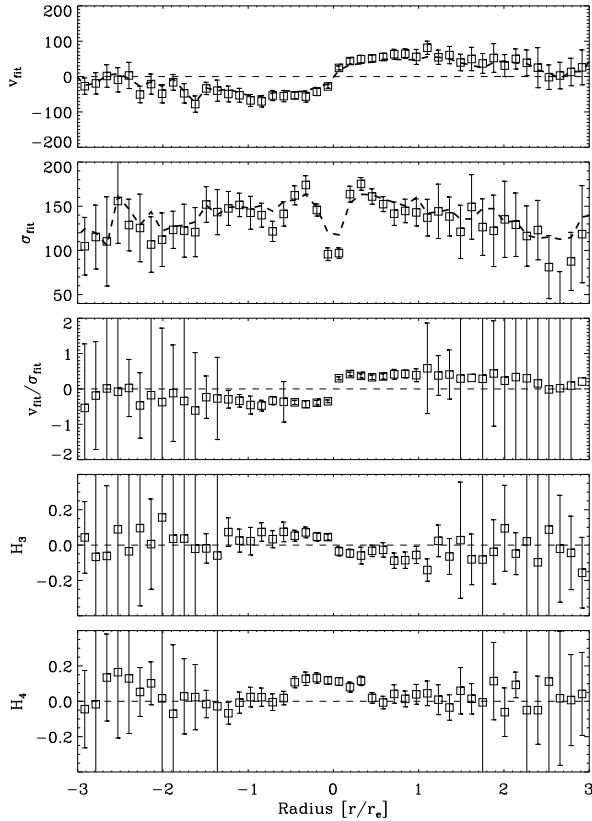


FIG. 12.— Analysis of the LOSVD of galaxy A as measured along a slit aligned with the major axis of the moment of inertia tensor of the main stellar body (open squares). The fitted local velocity v_{fit} , local velocity dispersion σ_{fit} , $v_{\text{rot}}/\sigma_{\text{fit}}$, H_3 , and H_4 are plotted versus radius. The dashed lines show the true line-of-sight velocity and dispersion, respectively. The individual error-bars were derived by bootstrapping.

computed the parameters for 500 random projections of each galaxy and show the area enclosing the 90% most likely observed data points. For comparison we show the observations for disk (diamonds) and boxy (squares) elliptical galaxies. All galaxies are similar to isotropic rotators (defined here as $\log(v_{\text{maj}}^*/\sigma_0) > 0.7$). Galaxy A is only marginally disk, Galaxy C can be very disk but also has some boxy projections, both are in good agreement with observations of disk and boxy isotropic ellipticals. Galaxy E has the largest values for $v_{\text{maj}}^*/\sigma_0$ and is extremely disk. It also show the largest values for rotational support $v_{\text{maj}}/\sigma_0 > 1$ (Fig. 15, right panel) whereas galaxy C shows smaller values $v_{\text{maj}}/\sigma_0 \approx 0.7$ and ellipticities as large as $\epsilon = 0.5$. Galaxy a has the lowest values of $v_{\text{maj}}/\sigma_0 \approx 0.2$ and is nearly round at $\epsilon = 0.2$.

In summary the high star-formation rate, the exponential surface brightness distribution, the kinematics and the isophotal shape of galaxy E makes it more similar to an early-type spiral galaxies. Galaxies A and C do resemble M_* elliptical galaxies. They follow the Fundamental Plane ($[\sigma_0, SB_e, r_e] = [153 \text{ km/s}, 20.5 \text{ mag arcsec}^{-2}, 2.7 \text{ kpc}]$; $[\sigma_0, SB_e, r_e] = [145 \text{ km/s}, 20.3 \text{ mag arcsec}^{-2}, 2.8 \text{ kpc}]$) (Bender et al. 1992) and are consistent with the observed $n - M_B$ and the $n - \sigma$ correlation (Trujillo et al. 2004).

6. DISCUSSION

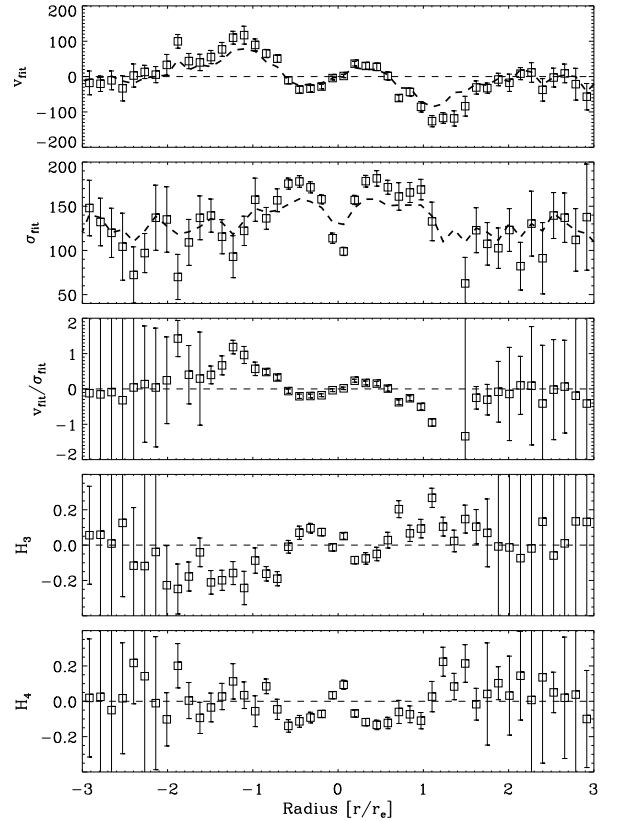


FIG. 13.— Sam as Fig. 12 for galaxy C. Note that this galaxy has a counter-rotating core with a radius of $\approx 0.5r_e$.

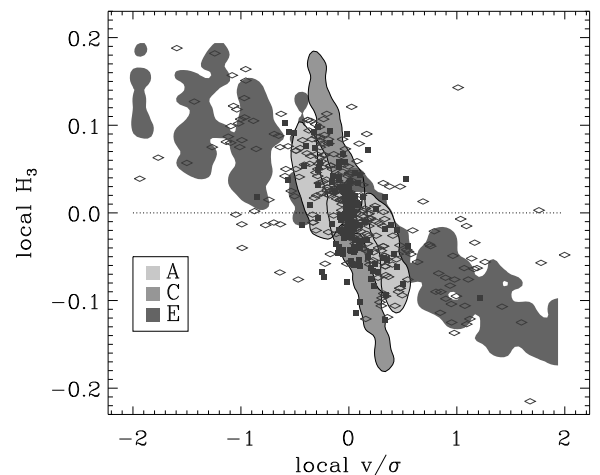


FIG. 14.— Local correlation between h_3 and v_{fit}/σ_0 for galaxies A, C, and E for 500 random projections. 90% of the data points cover the regions indicated by the shaded areas. The observed values for disk (open diamonds) and boxy ellipticals (filled boxes) are overplotted (Bender et al. 1994).

We have followed the formation and evolution of three $\approx M_*$ field galaxies using numerical simulations 'ab initio' from cosmological initial conditions at high redshift. All galaxies start to form when cold gas that has collapsed in subunits is effectively consumed by star formation. At early times the remaining diffuse gas is predominantly heated by shocks. In general the stars galaxies assemble both by in situ star formation as well as major/minor mergers and accretion. During the early

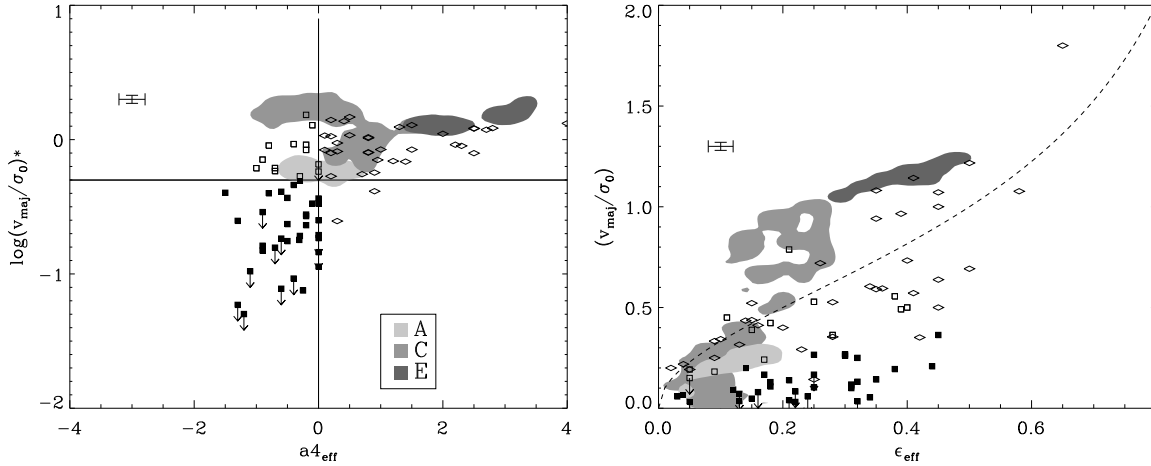


FIG. 15.— *Left panel:* Isophotal shape $a4_{\text{eff}}$ versus anisotropy parameter $(v_{\text{maj}}/\sigma_0)^*$. The contours indicate the 90% probability to find a simulated galaxy (seen from 500 random viewing angles) in the enclosed area. The horizontal line at $(v_{\text{maj}}/\sigma_0)^* = 0.5$ separates the anisotropic boxy from the more rotationally flattened disk and boxy ellipticals. *Right panel:* Ellipticity ϵ_{eff} versus the ratio of major axis rotation velocity and central velocity dispersion $(v_{\text{maj}}/\sigma_0)$. The data for observed disk (diamonds), very anisotropic boxy (filled boxes) and less anisotropic boxy (open boxes) ellipticals have been kindly provided by Ralf Bender. The properties of the galaxies are largely consistent with rotationally flattened disk and boxy ellipticals.

formation phase at $2 < z < 8$ the assembly of the galaxies is dominated by mergers of gas rich subcomponents and in situ star formation. Although some fraction of the stars is accreted this phase has the characteristics of a dissipative collapse. Thereafter stellar accretion or minor/major mergers become more important and, for early-type galaxies, tends to dominate for $z < 1$.

After $z=1$ the further assembly of the galaxies varies from halo to halo. The evolution of one galaxy is dominated by gas infall and in situ star formation at rates of $5-8M_{\odot}/\text{yr}$. It develops a massive, however too compact, stellar disk and has properties more similar to early-type disk galaxies.

Two other galaxies have present day properties more similar to elliptical galaxies and their assembly is dominated by minor and major predominantly stellar mergers. One of the galaxies grows by minor mergers and does not experience a major merger after its formation phase. At redshift $z \approx 1$ it has formed a massive stellar spheroid (see e.g. Nagamine et al. 2005) which resembles observed massive evolved galaxies and their inferred formation histories (Daddi et al. 2000). The system evolves into an old stellar system surrounded by a halo of hot gas at the present day. The second early-type galaxy had a major merger at $z=0.6$ that can be classified as a gas poor or 'dry' merger as it was not accompanied by a strong burst of star-formation. From those two examples we find that $\approx 15\% - 35\%$ of the final stellar mass was assembled by accretion of stars that have formed outside the galaxy (see Khochfar & Silk 2006b). This increase will contribute to the evolution of the luminosity function of elliptical galaxies from $z = 1 \rightarrow 0$ in addition to a fading population of blue galaxies and mergers (Bell et al. 2004; Drory et al. 2004; Conselice et al. 2005; Faber et al. 2005). The size evolution of the simulated early-type galaxies is determined by the accreted stars. While the half-mass radius of the stars formed in-situ remains almost constant independent of redshift at $r_{1/2} = 1 - 2$ kpc the accreted stars create an envelope whose half-mass radius is increasing with decreasing redshift (see Khochfar & Silk 2006a, for a semi-analytical

approach). Interestingly, a significant fraction of the stars at the final half-mass radius of the galaxies were not born there but accreted. This process might provide a good explanation for a possible size evolution of early-type galaxies (Trujillo et al. 2006; Longhetti et al. 2006) without changing the fundamental parameter relations which are determined by the central properties of the galaxies and should have been established during the early formation phase.

At the present day most investigated kinematical and photometric properties (see also Sommer-Larsen et al. 2003) are consistent with observed rotating disk and boxy early-type galaxies at similar luminosities. In particular, the concentration is in good agreement with observations. We believe that the discrepancy with Meza et al. (2003) is due to the different star formation algorithm which in their case allows predominantly gaseous subunits to merge and develop a high concentration before forming stars. In our simulations gas is converted into stars efficiently in subunits which merge at early times, prior to $z=2$, and so the morphology of the systems is elliptical if its late accretion is dominated by stars. Interestingly, the early-type galaxy with the late major merger develops a counter rotating core which previously only have been successfully simulated in isolated equal-mass disk-disk mergers (Hernquist & Barnes 1991; Jesseit et al. 2006) and are supposed to be signposts of merger events.

Feedback from supernovae and/or AGN, which was not included in this simulation, would provide additional heat sources but appear neither vital to stop the star formation and produce a massive red galaxy at higher redshifts nor to produce a present day stellar system with consistent kinematical properties. Theoretical arguments (see e.g. Dekel & Silk 1986; Efstathiou 2000) suggest that stellar feedback rapidly becomes ineffective in systems with velocity dispersions greater than 100 km/s. However, AGN feedback may be important in galaxies with high velocity dispersions (Silk & Rees 1998; Fabian 1999; Ciotti & Ostriker 2001). In our case AGN feedback might have been able to prevent further star formation

at low redshift by heating the cold gas at the center of the galaxy (see e.g. Springel et al. 2005a; Sazonov et al. 2005). On the other hand many field ellipticals show the related E+A phenomenon which seems to be suppressed in the centers of clusters as any residual cold gas will be blown away (Caldwell et al. 1993). For more massive systems than the ones studied here it has been argued that feedback from AGN might have a bigger impact and be responsible for the sharp cutoff at the bright end of the luminosity function of ellipticals (Croton et al. 2005). However, only full cosmological simulations at high resolution of the formation of more massive systems will help to fully understand the importance of stellar and AGN feedback on the formation and evolution of elliptical galaxies.

In a hierarchical universe most galaxies are expected to experience mergers but it has been argued for a long time that dissipation is essential to explain properties of elliptical galaxies and in particular intermediate mass ellipticals (Kormendy 1989 and references therein; Kormendy & Bender 1996; Naab et al. 2006a). The cosmological formation processes pre-

sented here combines characteristics of both stellar mergers and dissipational collapse/mergers whereas the latter dominates the early formation phase. It naturally meets many observational constraints on the evolution of massive spheroidal galaxies (e.g. Treu et al. 2005; Thomas et al. 2005a; van der Wel et al. 2005). It might be equally or even more important than major mergers of disk galaxies (Robertson et al. 2006; Hopkins et al. 2006) which can not reproduce the properties the most massive ellipticals (Naab & Burkert 2003; Cox et al. 2006) whose evolution could be driven by mergers of evolved ellipticals (Ostriker & Hausman 1977; Khochfar & Burkert 2003; Bell et al. 2006a; Naab et al. 2006b; Boylan-Kolchin et al. 2006).

We thank Volker Springel for making GADGET2 available prior to publication and Ralf Bender and Andy Fabian for discussions about the manuscript. We also thank the anonymous referee for valuable comments on the manuscript.

REFERENCES

- Abadi, M. G., Navarro, J. F., Steinmetz, M., & Eke, V. R. 2003, *ApJ*, 597, 21
- Agertz, O. et al. 2006, *ArXiv Astrophysics e-prints*
- Bell, E. F., McIntosh, D. H., Katz, N., & Weinberg, M. D. 2003, *ApJS*, 149, 289
- Bell, E. F. et al. 2006a, *ApJ*, 640, 241
- Bell, E. F., Phleps, S., Somerville, R. S., Wolf, C., Borch, A., & Meisenheimer, K. 2006b, *astro-ph/0602038*
- Bell, E. F. et al. 2004, *ApJ*, 608, 752
- Bender, R., Burstein, D., & Faber, S. M. 1992, *ApJ*, 399, 462
- Bender, R., Saglia, R. P., & Gerhard, O. E. 1994, *MNRAS*, 269, 785
- Birnboim, Y., & Dekel, A. 2003, *MNRAS*, 345, 349
- Blake, C. et al. 2004, *MNRAS*, 355, 713
- Blumenthal, G. R., Faber, S. M., Flores, R., & Primack, J. R. 1986, *ApJ*, 301, 27
- Bower, R. G., Kodama, T., & Terlevich, A. 1998, *MNRAS*, 299, 1193
- Boylan-Kolchin, M., Ma, C.-P., & Quataert, E. 2006, *MNRAS*, 369, 1081
- Brinchmann, J., & Ellis, R. S. 2000, *ApJ*, 536, L77
- Bruzual, G., & Charlot, S. 2003, *MNRAS*, 344, 1000
- Bullock, J. S., Dekel, A., Kolatt, T. S., Kravtsov, A. V., Klypin, A. A., Porciani, C., & Primack, J. R. 2001, *ApJ*, 555, 240
- Butcher, H., & Oemler, Jr., A. 1978, *ApJ*, 219, 18
- Caldwell, N., Rose, J. A., Sharples, R. M., Ellis, R. S., & Bower, R. G. 1993, *AJ*, 106, 473
- Ciotti, L., & Ostriker, J. P. 2001, *ApJ*, 551, 131
- Cole, S. et al. 2001, *MNRAS*, 326, 255
- Conselice, C. J., Blackburne, J. A., & Papovich, C. 2005, *ApJ*, 620, 564
- Couchman, H. M. P. 1991, *ApJ*, 368, L23
- Cox, T. J., Dutta, S. N., Di Matteo, T., Hernquist, L., Hopkins, P. F., Robertson, B., & Springel, V. 2006, *astro-ph/0607446*
- Croton, D. J. et al. 2005, *MNRAS*, 356, 1155
- Daddi, E., Cimatti, A., & Renzini, A. 2000, *A&A*, 362, L45
- Davé, R., Hernquist, L., Katz, N., & Weinberg, D. H. 1999, *ApJ*, 511, 521
- Dekel, A., & Birnboim, Y. 2006, *MNRAS*, 368, 2
- Dekel, A., & Silk, J. 1986, *ApJ*, 303, 39
- Dressler, A. 1980, *ApJ*, 236, 351
- Drory, N., Bender, R., Feulner, G., Hopp, U., Maraston, C., Snigula, J., & Hill, G. J. 2004, *ApJ*, 608, 742
- Efstathiou, G. 2000, *MNRAS*, 317, 697
- Efstathiou, G., Bond, J. R., & White, S. D. M. 1992, *MNRAS*, 258, 1P
- Efstathiou, G., Ellis, R. S., & Carter, D. 1982, *MNRAS*, 201, 975
- Emsellem, E. et al. 2004, *MNRAS*, 352, 721
- Faber, S. M. et al. 2005, *astro-ph/0506044*
- Fabian, A. C. 1999, *MNRAS*, 308, L39
- Fukugita, M., Hogan, C. J., & Peebles, P. J. E. 1998, *ApJ*, 503, 518
- Gerhard, O. E. 1993, *MNRAS*, 265, 213
- Governato, F. et al. 2004, *ApJ*, 607, 688
- Haardt, F., & Madau, P. 1996, *ApJ*, 461, 20
- Hernquist, L., & Barnes, J. E. 1991, *Nature*, 354, 210
- Hopkins, P. F., Hernquist, L., Cox, T. J., Di Matteo, T., Robertson, B., & Springel, V. 2006, *ApJS*, 163, 1
- Jesseit, R., Naab, T., & Burkert, A. 2002, *ApJ*, 571, L89
- Jesseit, R., Naab, T., Peletier, R., & Burkert, A. 2006, *astro-ph/0606144*
- Junk, V. J., Naab, T. N., Heitsch, F. H., & Wetzstein, M. W. 2006, in *IAU Symposium*
- Katz, N., Weinberg, D. H., & Hernquist, L. 1996, *ApJS*, 105, 19
- Kaviraj, S., Devriendt, J. E. G., Ferreras, I., & Yi, S. K. 2005, *MNRAS*, 360, 60
- Kawata, D., & Gibson, B. K. 2003, *MNRAS*, 346, 135
- Khochfar, S., & Burkert, A. 2003, *ApJ*, 597, L117
- . 2005, *MNRAS*, 359, 1379
- Khochfar, S., & Silk, J. 2006a, *ApJ*, 648, L21
- . 2006b, *MNRAS*, 370, 902
- Kobayashi, C. 2004, *MNRAS*, 347, 740
- Kochanek, C. S. et al. 2001, *ApJ*, 560, 566
- Kormendy, J. 1989, *ApJ*, 342, L63
- Kormendy, J., & Bender, R. 1996, *ApJ*, 464, L119+
- Larson, R. B. 1974, *MNRAS*, 169, 229
- Longhetti, M. et al. 2006, *ArXiv Astrophysics e-prints*
- McCarthy, P. J. 2004, *ARA&A*, 42, 477
- McIntosh, D. H., Zabludoff, A. I., Rix, H.-W., & Caldwell, N. 2005, *ApJ*, 619, 193
- Meza, A., Navarro, J. F., Steinmetz, M., & Eke, V. R. 2003, *ApJ*, 590, 619
- Moore, B., Governato, F., Quinn, T., Stadel, J., & Lake, G. 1998, *ApJ*, 499, L5+
- Moustakas, L. A. et al. 2004, *ApJ*, 600, L131
- Naab, T., & Burkert, A. 2003, *ApJ*, 597, 893
- Naab, T., Jesseit, R., & Burkert, A. 2006a, *MNRAS*, 372, 839
- Naab, T., Khochfar, S., & Burkert, A. 2006b, *ApJ*, 636, L81
- Naab, T., & Trujillo, I. 2006, *MNRAS*, 369, 625
- Nagamine, K., Cen, R., Hernquist, L., Ostriker, J. P., & Springel, V. 2005, *ApJ*, 618, 23
- Navarro, J. F., & White, S. D. M. 1993, *MNRAS*, 265, 271
- Ostriker, J. P., & Hausman, M. A. 1977, *ApJ*, 217, L125
- Rakos, K. D., & Schombert, J. M. 1995, *ApJ*, 439, 47
- Rix, H.-W., de Zeeuw, P. T., Cretton, N., van der Marel, R. P., & Carollo, C. M. 1997, *ApJ*, 488, 702
- Robertson, B., Cox, T. J., Hernquist, L., Franx, M., Hopkins, P. F., Martini, P., & Springel, V. 2006, *ApJ*, 641, 21

- Robertson, B., Yoshida, N., Springel, V., & Hernquist, L. 2004, *ApJ*, 606, 32
- Romanowsky, A. J., Douglas, N. G., Arnaboldi, M., Kuijken, K., Merrifield, M. R., Napolitano, N. R., Capaccioli, M., & Freeman, K. C. 2003, *Science*, 301, 1696
- Sáiz, A., Domínguez-Tenreiro, R., & Serna, A. 2004, *ApJ*, 601, L131
- Sazonov, S. Y., Ostriker, J. P., Ciotti, L., & Sunyaev, R. A. 2005, *MNRAS*, 358, 168
- Schawinski, K. et al. 2006, arXiv:astro-ph/0601036
- Searle, L., Sargent, W. L. W., & Bagnuolo, W. G. 1973, *ApJ*, 179, 427
- Silk, J., & Rees, M. J. 1998, *A&A*, 331, L1
- Sommer-Larsen, J., Götz, M., & Portinari, L. 2003, *ApJ*, 596, 47
- Spiegel, D. N. et al. 2003, *ApJS*, 148, 175
- Springel, V. 2005, *MNRAS*, 364, 1105
- Springel, V., Di Matteo, T., & Hernquist, L. 2005a, *ApJ*, 620, L79
- Springel, V., & Hernquist, L. 2003, *MNRAS*, 339, 289
- Springel, V. et al. 2005b, *Nature*, 435, 629
- Susa, H., & Umemura, M. 2000, *ApJ*, 537, 578
- Thomas, D., Maraston, C., Bender, R., & de Oliveira, C. M. 2005a, *ApJ*, 621, 673
- Thomas, J., Saglia, R. P., Bender, R., Thomas, D., Gebhardt, K., Magorrian, J., Corsini, E. M., & Wegner, G. 2005b, *MNRAS*, 360, 1355
- Tran, K.-V. H., van Dokkum, P., Franx, M., Illingworth, G. D., Kelson, D. D., & Schreiber, N. M. F. 2005, *ApJ*, 627, L25
- Treu, T. et al. 2005, *ApJ*, 633, 174
- Treu, T., & Koopmans, L. V. E. 2004, *ApJ*, 611, 739
- Trujillo, I., Burkert, A., & Bell, E. F. 2004, *ApJ*, 600, L39
- Trujillo, I. et al. 2006, *ApJ*, 650, 18
- Väisänen, P., & Johansson, P. H. 2004, *A&A*, 421, 821
- van Albada, T. S. 1982, *MNRAS*, 201, 939
- van der Marel, R. P., & Franx, M. 1993, *ApJ*, 407, 525
- van der Wel, A., Franx, M., van Dokkum, P. G., Rix, H.-W., Illingworth, G. D., & Rosati, P. 2005, *ApJ*, 631, 145
- van Dokkum, P. G. 2005, *AJ*, 130, 2647
- Vitvitska, M., Klypin, A. A., Kravtsov, A. V., Wechsler, R. H., Primack, J. R., & Bullock, J. S. 2002, *ApJ*, 581, 799
- Zheng, Z., & Miralda-Escudé, J. 2002, *ApJ*, 568, L71